Supporting Information

Tough and anti-freezing organohydrogel electrolyte for flexible supercapacitor with wide-temperature stability

*Jiwei Chen‡, Qiuyan Yu‡, Dongjian Shi, Zhaokun Yang, Kaijie Dong, Daisaku Kaneko, Weifu Dong and Mingqing Chen**

The Key Laboratory of Synthetic and Biological Colloids, Ministry of Education, School of Chemical and Material Engineering, Jiangnan University, Wuxi, Jiangsu 214122, China.

Corresponding email: mqchen@jiangnan.edu.cn

[‡] These authors contributed equally to this work.

1.1. CHARACTERIZATION

Field emission scanning electron microscope (SEM) measurements. Field emission scanning electron microscope (SEM) measurements of the freeze-drying hydrogels and organohydrogels were performed on an S-4800 (Hitachi, Japan) under an accelerating voltage of 15 kV. Since the organohydrogels cannot be froze by traditional freeze-drying method, in this work, the hydrogels and organohydrogels were first soaked in an aqueous solution composed of glutaraldehyde, hydrochloric acid and distilled water (volume ratio = 20:1:50) for 2 h to fix the network structure of the samples[1]. Then, they were soaked in distilled water for 12 h to remove the residual hydrochloric acid, $CaCl_2$ and organic molecules. Finally, the hydrogels were freeze-dried and then stuck on the copper plate for the SEM measurements.

Attenuated total reflectance Fourier transform infrared spectrometry (ATR-FTIR) measurements. Attenuated total reflectance Fourier transform infrared spectra (ATR-FTIR) of the obtained hydrogels and organohydrogels were detected on a Nicolet iS50 FT-IR (Thermo Fisher Scientific, American) in the range of 750-4000 cm^{-1} with a nominal resolution of 4 cm^{-1}. Each spectrum repetitiously scanned 16 times to get an averaged value.

Thermogravimetric analysis (TGA) tests. Thermogravimetric analysis (TGA) of the hydrogels and organohydrogels were performed using a TGA/1100SF instrument (Mettler-Toledo, Switzerland) and recorded at a ramp rate of 10 ℃ min^{-1} up to 600 ℃

under N_2 flow.

Characterization of water-holding capacity. Water-holding capacity content experiments were performed by putting the sample with the mass m_1 in a vacuum oven at 60 ℃ for 24 h until the mass of the sample without change to obtain the mass m_2. Then, the water-holding capacity of the sample was evaluated from the following equation and averaged from three tests:

Water content = $(m_1 - m_2) / m_2 \times 100\%$ (Equation S1)

Differential scanning calorimetry (DSC) characterization. A differential scanning calorimeter (DSC, NETZSCH-Gerätebau GmbH, model: 204 F1) was used for the characterization of the anti-freezing properties of the different samples. The scan of the samples was performed from 20 to -80 ℃ at a cooling rate of 10 ℃ min^{-1}.

Rheological characterization. Rheological properties were tested by using a plate-to-plate type rheometer, DHR-1 (TA Instruments) equipped with 8 mm of diameter stainless steel parallel plate geometry at 25 ℃. Dynamic strain sweep was conducted prior to the frequency sweep, and strain was determined to be 1% to ensure the rheological measurements within a linear viscoelastic range. The range of the shear frequency is from 1 to 100 rad/s to determine the storage and loss moduli of the hydrogels and organohydrogels. The tests were started as soon as the samples were prepared to prevent moisture evaporation. Each test was replicated three times.

Mechanical measurement. The mechanical tests were performed on a universal

double column bench testing machine (5967X, ITW Company, American) in air with 40% humidity at room temperature. The samples were cut into a dumbbell-shaped (15 mm in length and 4 mm in width) were used for the tensile tests at a speed of 50 mm min^{-1}. The strain of the sample was calculated as the length change related to the initial length, and the stress was estimated by dividing the force by the initial cross-sectional area of the hydrogel. The elastic modulus was obtained using the slope of the initial linear region of the stress-strain curve. Five samples were tested for each group. For the cyclic loading and unloading measurements, the sample was stretched to a certain extension ratio, and then unloaded at the speed of 50 mm min^{-1}. The dissipated energy is the area of the cyclic loading-unloading curve.

Electrochemical measurements. The ionic conductivities of the hydrogels and oranohydrogels were performed by AC impedance technique. The rectangular electrolyte samples were sandwiched between two stainless steel electrodes and ensured firm contact. The measurements by CHI 660E (CH Instruments, Inc.) were set in the frequency range of 0.01 Hz to 100 kHz. The bulk resistance of the sample electrolyte (R) was the intersection of the curve at the real part, and the ionic conductivity of the sample was calculated according to the following equation:

$$\rho = L / (S \times R) \qquad \text{(Equation S2)}$$

where L is the thickness of the sample electrolyte and S is the electrode area.

The electrochemical performance of the all-in-one flexible organohydrogel supercapacitor was investigated on a CHI 660E electrochemical workstation

(Chenhua CHI 660E). The CV tests of the supercapacitor was carried out at the potentials of 0.6-1.2 V at the scanning rates of 20-300 mV s^{-1}. Galvanostatic charge-discharge (GCD) was tested with different current densities at 0.5-1.5 mA cm^{-2}. The specific capacitance (C_{sp}, mF cm^{-2}) could be calculated from discharge curves according to the following equations [2, 3]:

$C_{SP} = (I \times \Delta t) / (S \times \Delta V)$ (Equation S3)

where I (A) is the current, ΔV (V) is the potential window, S (cm^2) is the area of the all-in-one flexible organohydrogel supercapacitor, and Δt (s) is the discharge time.

Volumetric energy density (E), and power density (P) of the devices are calculated according to the following equations:

$E = (C_{SP} \times V^2) / (2 \times 3.6)$ (Equation S4)

$P = (E \times 3600) / \Delta t$ (Equation S5)

Table S1 Proportions and properties of different samples.

Samples (PA-x-y)	$CaCl_2$ concentration (mol L^{-1})	Soaking step: Ratio of organic molecules and water (V:V)
PA-DI	0	--
PA-Ca	1	--
PA-EG	0	1:2
PA-Gly	0	1:3
PA-Sor	0	/
PA-EG-Ca	1	1:2
PA-Gly-Ca	1	1:3
PA-Sor-Ca	1	/

--: Without glycerol.

/: the concentration of sorbitol is 2.285 mol L^{-1}.

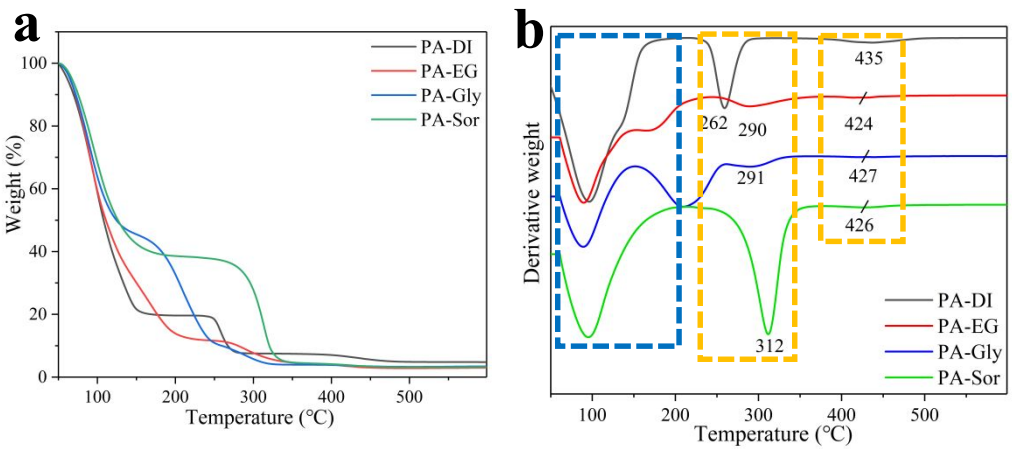

Figure S1. (a) TGA and (b) DTG curves of the PA-DI hydrogels and the PA-EG, PA-Gly, and PA-Sor organohydrogels prepared by PVA/Alg pre-hydrogel soaking deionized water or water/organic

molecules (ethylene glycol, glycerol, or sorbitol) binary solution.

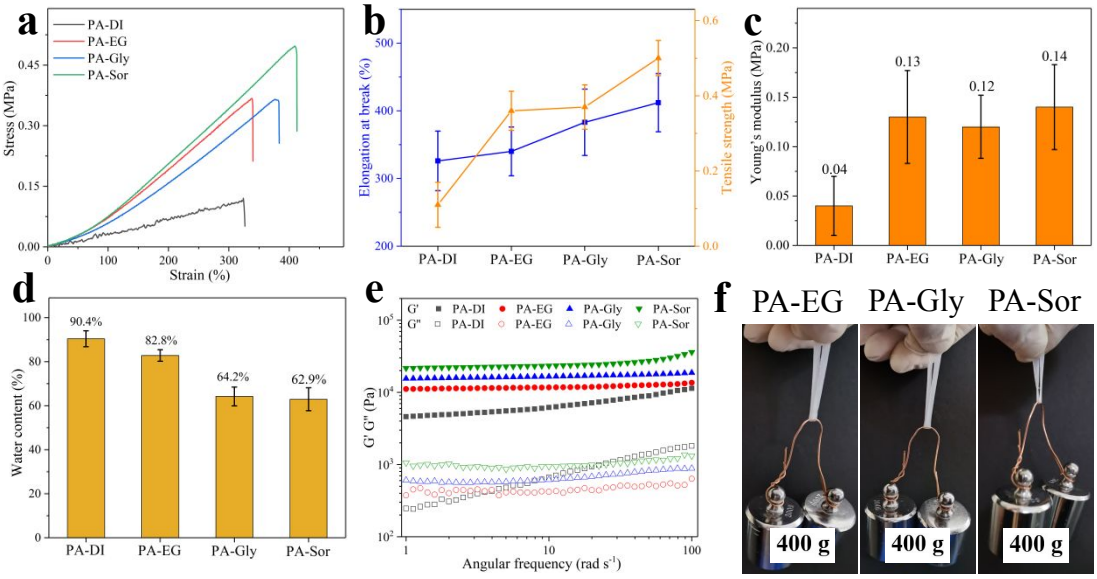

Figure S2. (a) Tensile stress–strain curves, (b) elongation at break and tensile strength, (c) Young's modulus, (d) rheological, and (e) water contents of PVA/Alg pre-hydrogel soaking deionized water or water/bridge molecules (ethylene glycol, glycerol, or sorbitol) solution. (f) Digital images of the PA-EG, PA-Gly, and PA-Sor organohydrogel (4 mm×2 mm) can supporting a 400 g weight.

Figure S2 a-c showed the tensile stress-strain of the organohydrogels prepared by soaking the pre-hydrogel in the water/bridge molecules solution without $CaCl_2$. Compared with the sample soaked in distilled water, the tensile strength, elongation at break and the Young's modulus of the organohydrogels all improved slightly, which inferred that the binary and polyol as the bridge molecules crosslinked the PVA and Alg chains by forming multiple hydrogen bonds, thereby increasing the strength of the organohydrogel. The crosslinked structures of the organohydrogels more compact with the increasement of the hydroxyl groups in the bridge molecules, therefore the water content of the organohydrogel decreased (Figure S2d) and the strength

increased (Figure S2b and c). Similar with the CNOHs, G′ of the organohydrogels was also much greater than G″, and G′ and G″ of the organohydrogels were greater than those of PA-DI (Figure S2e), indicating the well mechanical properties (Figure S2f). However, due to the lack of the effective energy dissipation network structure (the rigid Alg-Ca ionic bonds) in the organohydrogels, the mechanical performance of the organohydrogels was very poor compared with that of the CNOHs.

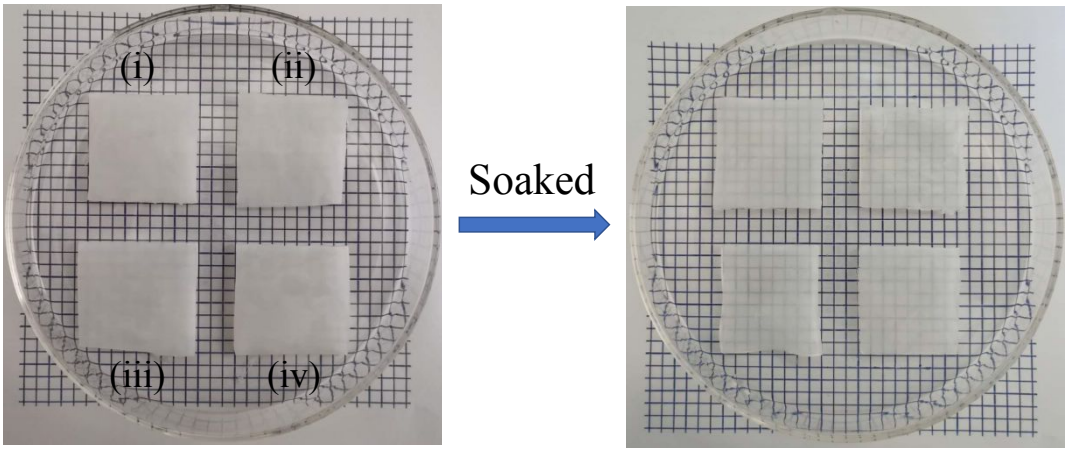

Figure S3. Digital images of PVA/Alg pre-hydrogels before and after soaking in 1 M $CaCl_2$ solution in (i) water, (ii) ethylene glycol/water solution, (iii) glycerol/water solution, and (iv) sorbitol/water solution for 7 h.

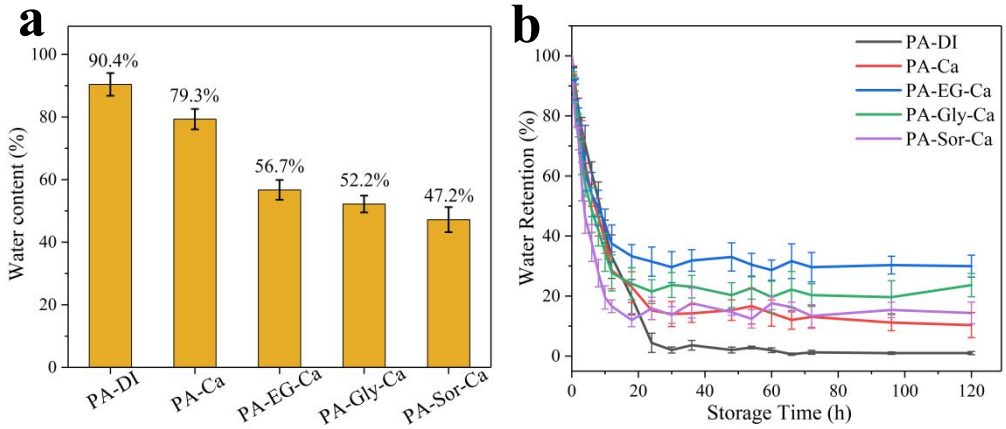

Figure S4. (a) Water contents of the PA-DI, PA-Ca, PA-EG-Ca, PA-Gly-Ca, and PA-Sor-Ca samples. (b) Water retention rate of the PA-DI, PA-Ca, PA-EG-Ca, PA-Gly-Ca, and PA-Sor-Ca exposed in air.

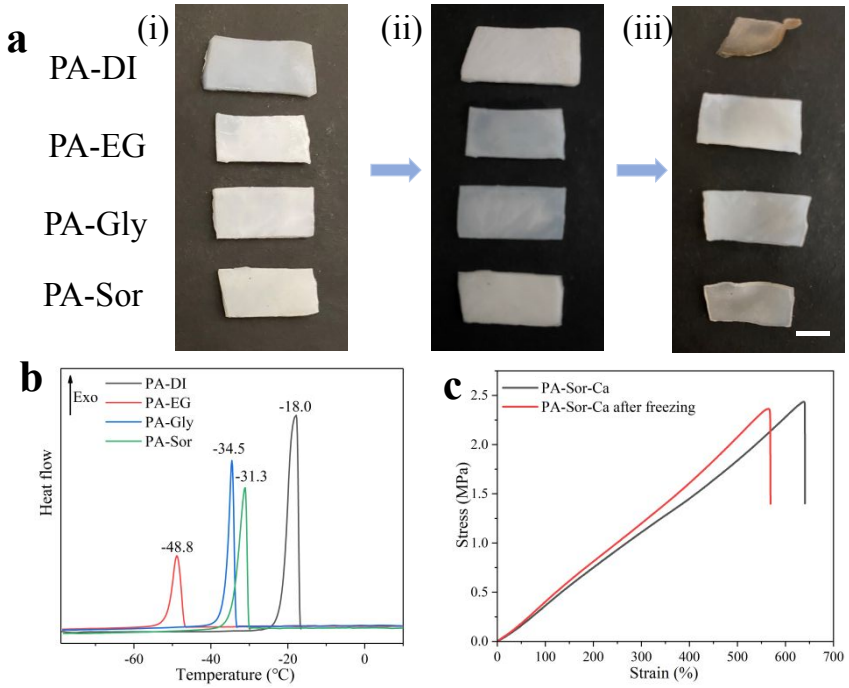

Figure S5. (a) Digital images of organohydrogels PA-DI, PA-EG, PA-Gly, and PA-Sor stored at (i) ambient conditions, (ii) -20 ℃ for 24 h, and (iii) in air 72 h. (b) DSC curves of the PA-DI, PA-EG, PA-Gly, and PA-Sor, (c) tensile stress–strain curves of PA-Gly-Ca before and after stored at -20 ℃ for 24 h. Scale bar is 1 cm.

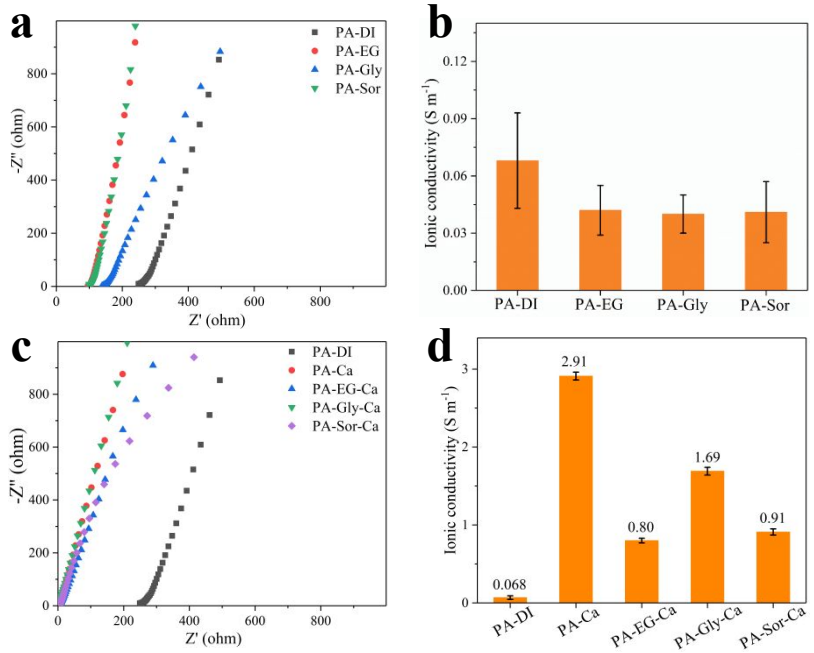

Figure S6. Nyquist plots (a and c) and calculated conductivity (b and d) of the as-prepared hydrogels and organohydrogels.

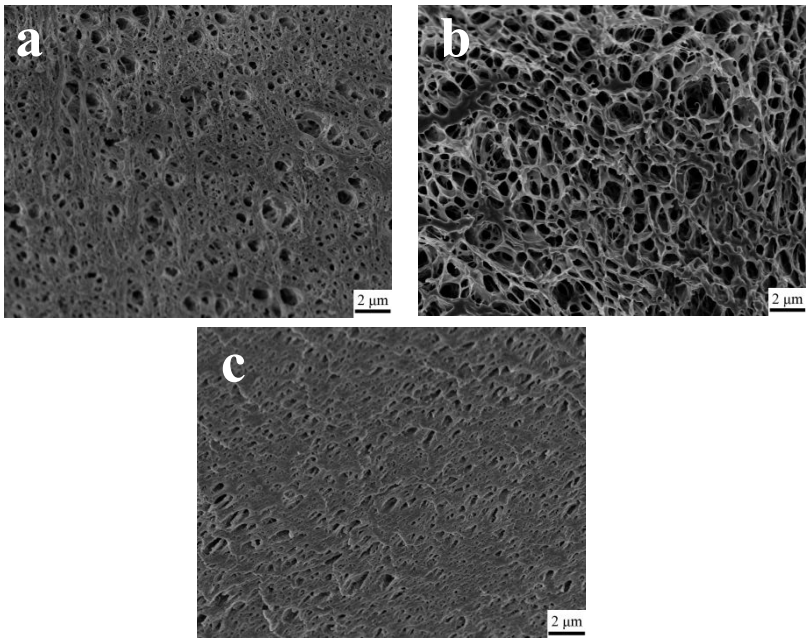

Figure S7. SEM images of (a) the PA-EG-Ca, (b) the PA-Gly-Ca, and (c) the PA-Sor-Ca CNOHs.

Table S2 Comparison of ionic conductivity of hydrogels/organohydrogels electrolytes

Hydrogels/ Organohydrogels	Solvent	Ionic conductivity ρ/(S m^{-1})	References
PVA-g-PSBMA[a]	Water	0.84	Ref. 4
PAMPS-PAHz-PAAm[b]	Water	0.66	Ref. 5
PAAm	EG/Water	1.3 (-30 ℃)	Ref. 6
PAA-PC-LiOTf[c]	Water	0.75	Ref. 7
PAAm/Alg	Water	1.49	Ref. 8
HPC[d]/PVA	Gly/Water	0.57	Ref. 9
PVA-MA[e]/PAAm	EG/Water	0.48 (-40 ℃)	Ref. 10
PAAm/DMAPS	Water	0.85	Ref. 11
PA-Gly-Ca	Glycerol/Water	1.69	this work

a. PVA-g-PSBMA: poly(vinyl alcohol)-graft-poly(sulfobetaine methacrylate)

b. PAMPS-PAHz-PAAm: poly(2-Acrylamido-2-methyl-1-propanesulfonic acid)-polyacryloyl hydrazide-polyacrylamide

c. PAA-PC-LiOTf: Polyacrylic acid-polymer cement-lithium trifluoromethanesulfonate

d. HPC: hydroxypropyl cellulose

e. PVA-MA: methacrylate-functionalized PVA

f. DMAPS: 3-dimethyl(methacryloyloxyethyl) ammonium propane sulfonate

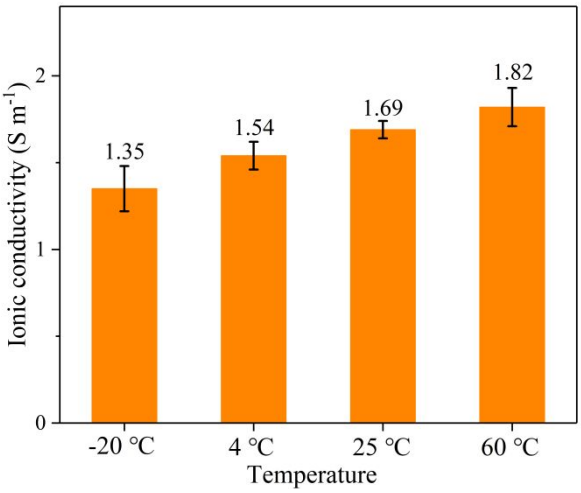

Figure S8. The ionic conductivity of the CNOH PA-Gly-Ca after stored at different temperatures 5 h.

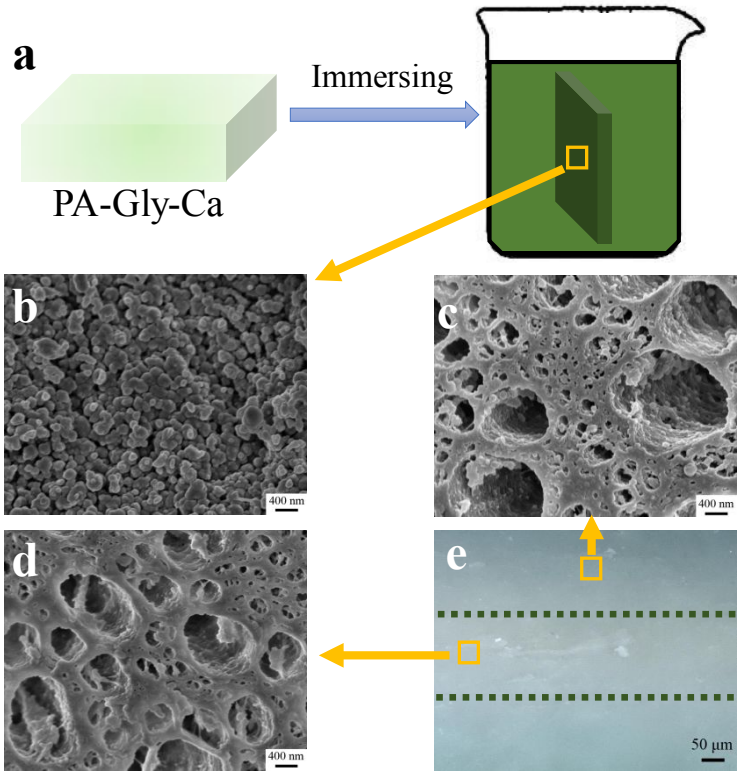

Figure S9. (a) Synthetic procedure of the PANI-decorated CNOH electrolyte. SEM images of the (b) surface and (c and d) cross-section of the PANI-decorated CNOH electrolyte. (e) The picture of the cross-section of the PANI-decorated CNOH electrolyte obtained from optical microscope.

When immersed the PA-Gly-Ca into the blended solution containing aniline, phytic

acid and APS, the nanocomposites electrode materials of PANI could be firmly in-situ polymerized and deposited onto the two-sided faces of the CNOH electrolyte separator, as shown in Figure S9a. SEM and optical microscopy were used to observe the surface and cross-section structure of the PANI-decorated CNOH electrolyte (Figure S9b-e). The uniform PANI nanoparticles on the surface of the CNOH electrolyte provided a good path for the electron transmission (Figure S9b). And the optical microscopy in Figure S10e displayed the cross-section of the PANI-decorated CNOH electrolyte, which could observe the obvious three layers from the clear color changes and the clear interface. The SEM images at different positions of the cross-section demonstrated the polymerization of PANI on the surface of the CNOH electrolyte, and the PANI gradually diffused into the CNOH electrolyte to form entanglements with the polymer networks (Figure S9c), which improved the contact area of the PANI electrode and CNOH electrolyte. Importantly, no PANI was observed in the middle of the CNOH electrolyte (Figure S9d), ensuring the function of the CNOH electrolyte as separator. The configured AFSC was assembled from cutting the edges of the bilateral nanocomposite electrode materials-coated CNOH electrolyte separator to avoid the short circuit and using the carbon cloth as the current collectors to connect the two opposite ends.

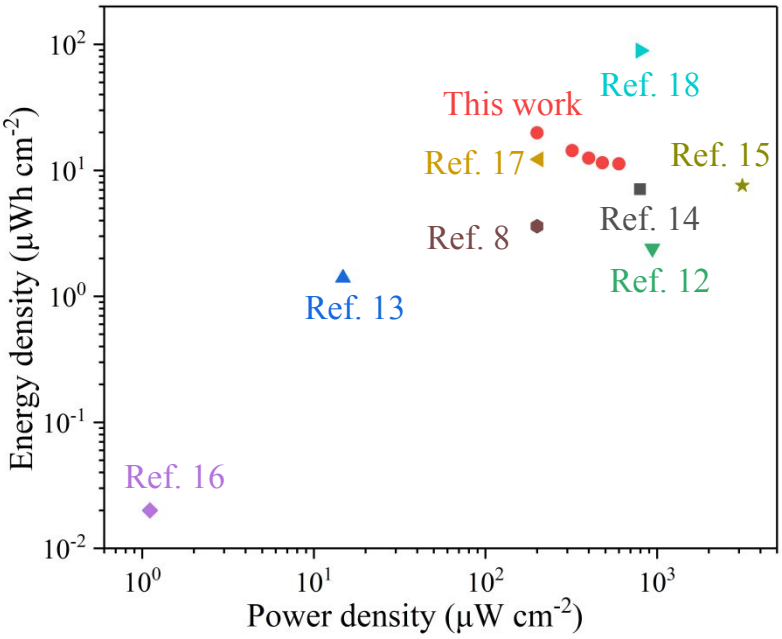

Figure S10. Ragone plot of the all-in-one flexible organohydrogel supercapacitor device compared with previously reported all-in-one supercapacitors based on our sample: PAAm/Alg/Na_2SO_4[8], PVA/PAA/H_2SO_4[12], PVA/H_2SO_4[13], PVA/PHEA/H_2SO_4[14], PVA/Phytic acid[15], PAA/H_3PO_4[16], PAA/H_2SO_4[17], and β-CD-g-Cell/H_2SO_4[18] as electrolyte.

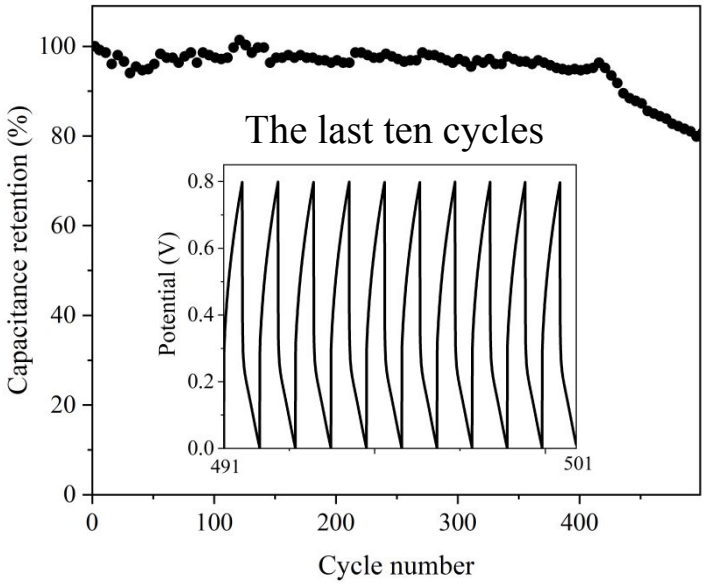

Figure S11. Cycling stability of the AFSC at 1.0 mA cm^{-2} (Inset: GCD curves of the last 5 cycles).

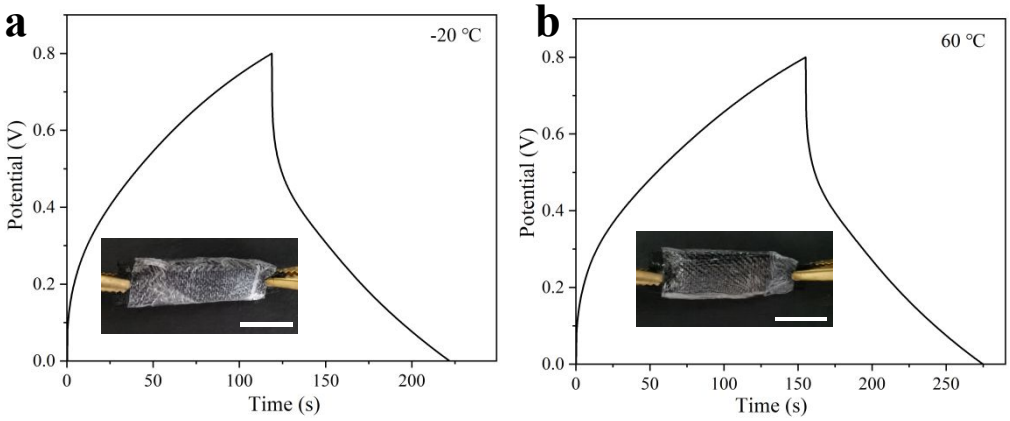

Figure S12. GCD curves of the AFSC at 1.0 mA cm^{-2} after stored at (a) -20 ℃ or (b) 60 ℃ for 5 h. (Inset: Digital images of AFSC after stored at (a) -20 ℃ or (b) 60 ℃ for 5 h. Scale bar is 1 cm.)

Reference

1. Lin, S.; Liu, X.; Liu, J.; Yuk, H.; Loh, H.-C.; Parada, G. A.; Settens, C.; Song, J.; Masic, A.; McKinley, G. H.; Zhao, X., Anti-fatigue-fracture hydrogels. *Sci. Adv.* **2019,** *5* (1), 8528.

2. Yang, Z.; Ma, J.; Bai, B.; Qiu, A.; Losic, D.; Shi, D.; Chen, M., Free-standing PEDOT/polyaniline conductive polymer hydrogel for flexible solid-state supercapacitors. *Electrochim. Acta* **2019,** *322*, 134769.

3. Yuan, H.; Wang, Y.; Li, T.; Ma, P.; Zhang, S.; Du, M.; Chen, M.; Dong, W.; Ming, W., Highly thermal conductive and electrically insulating polymer composites based on polydopamine-coated copper nanowire. *Compos. Sci. Technol.* **2018,** *164*, 153-159.

4. Min, H. J.; Park, M. S.; Kang, M.; Kim, J. H., Excellent film-forming, ion-conductive, zwitterionic graft copolymer electrolytes for solid-state supercapacitors. *Chem. Eng. J.* **2021,** *412*, 127500.

5. Mandal, S.; Kumari, S.; Kumar, M.; Ojha, U., Supplementary Networking of Interpenetrating Polymer System (SNIPSy) Strategy to Develop Strong & High Water Content Ionic Hydrogels for Solid Electrolyte Applications. *Adv. Funct. Mater.* **2021,** *n/a* (n/a), 2100251.

6. Jin, X.; Song, L.; Yang, H.; Dai, C.; Xiao, Y.; Zhang, X.; Han, Y.; Bai, C.; Lu, B.; Liu, Q.; Zhao, Y.; Zhang, J.; Zhang, Z.; Qu, L., Stretchable supercapacitor at −30 °C. *Energy & Environmental Science* **2021**.

7. Fang, C.; Zhang, D., High areal energy density structural supercapacitor assembled with polymer cement electrolyte. *Chem. Eng. J.* **2021,** *426*, 130793.

8. Zeng, J.; Dong, L.; Sha, W.; Wei, L.; Guo, X., Highly stretchable, compressible and arbitrarily deformable all-hydrogel soft supercapacitors. *Chem. Eng. J.* **2020,** *383*, 123098.

9. Lu, N.; Na, R.; Li, L.; Zhang, C.; Chen, Z.; Zhang, S.; Luan, J.; Wang, G., Rational Design of Antifreezing Organohydrogel Electrolytes for Flexible Supercapacitors. *ACS Appl. Energy Mater.* **2020,** *3* (2), 1944-1951.

10. Liu, Z.; Zhang, J.; Liu, J.; Long, Y.; Fang, L.; Wang, Q.; Liu, T., Highly compressible and superior low temperature tolerant supercapacitors based on dual chemically crosslinked PVA hydrogel electrolytes. *J. Mater. Chem. A* **2020,** *8* (13), 6219-6228.
11. Wei, J.; Wei, G.; Shang, Y.; Zhou, J.; Wu, C.; Wang, Q., Dissolution–Crystallization Transition within a Polymer Hydrogel for a Processable Ultratough Electrolyte. *Adv. Mater.* **2019,** *31* (30), 1900248.
12. Yu, H.; Rouelle, N.; Qiu, A.; Oh, J.-A.; Kempaiah, D. M.; Whittle, J. D.; Aakyiir, M.; Xing, W.; Ma, J., Hydrogen Bonding-Reinforced Hydrogel Electrolyte for Flexible, Robust, and All-in-One Supercapacitor with Excellent Low-Temperature Tolerance. *ACS Appl. Mater. Interfaces* **2020,** *12* (34), 37977-37985.
13. Guo, Y.; Zheng, K.; Wan, P., A Flexible Stretchable Hydrogel Electrolyte for Healable All-in-One Configured Supercapacitors. *Small* **2018,** *14* (14), e1704497.
14. Yang, J.; Yu, X.; Sun, X.; Kang, Q.; Zhu, L.; Qin, G.; Zhou, A.; Sun, G.; Chen, Q., Polyaniline-Decorated Supramolecular Hydrogel with Tough, Fatigue-Resistant, and Self-Healable Performances for All-In-One Flexible Supercapacitors. *ACS Appl. Mater. Interfaces* **2020,** *12* (8), 9736-9745.
15. Wang, Y.; Lv, C.; Ji, G.; Hu, R.; Zheng, J., An all-in-one supercapacitor with high stretchability via a facile strategy. *J. Mater. Chem. A* **2020,** *8* (17), 8255-8261.
16. Hu, M.; Wang, J.; Liu, J.; Zhang, J.; Ma, X.; Huang, Y., An intrinsically compressible and stretchable all-in-one configured supercapacitor. *Chem. Commun.* **2018,** *54* (48), 6200-6203.
17. Wang, H.; Dai, L.; Chai, D.; Ding, Y.; Zhang, H.; Tang, J., Recyclable and tear-resistant all-in-one supercapacitor with dynamic electrode/electrolyte interface. *J. Colloid Interface Sci.* **2020,** *561*, 629-637.
18. Gong, Q.; Li, Y.; Liu, X.; Xia, Z.; Yang, Y., A facile preparation of polyaniline/cellulose hydrogels for all-in-one flexible supercapacitor with remarkable enhanced performance. *Carbohydr. Polym.* **2020,** *245*, 116611.